



Article

Allosteric Binding Sites of A β Peptides on the Acetylcholine Synthesizing Enzyme ChAT as Deduced by In Silico Molecular Modeling

Anurag TK Baidya ^{1,†}, Amit Kumar ^{2,†}, Rajnish Kumar ^{1,2,*}  and Taher Darreh-Shori ^{2,*}

¹ Department of Pharmaceutical Engineering & Technology, Indian Institute of Technology (B.H.U.), Varanasi 221005, Uttar Pradesh, India; anuragtkbaidya.rs.phe20@itbhu.ac.in

² Division of Clinical Geriatric, Center for Alzheimer Research, Department of Neurobiology, Care Sciences and Society, Karolinska Institutet, NEO, 141 52 Stockholm, Sweden; amit.kumar@ki.se

* Correspondence: rajnish.phe@itbhu.ac.in (R.K.); taher.darreh-shori@ki.se (T.D.-S.)

† These authors contributed equally to this work.

Abstract: The native function of amyloid- β (A β) peptides is still unexplored. However, several recent reports suggest a prominent role of A β peptides in acetylcholine homeostasis. To clarify this role of A β , we have reported that A β peptides at physiological concentrations can directly enhance the catalytic efficiency of the key cholinergic enzyme, choline acetyltransferase (ChAT), via an allosteric interaction. In the current study, we further aimed to elucidate the underlying ChAT-A β interaction mechanism using in silico molecular docking and dynamics analysis. Docking analysis suggested two most probable binding clusters on ChAT for A β_{40} and three for A β_{42} . Most importantly, the docking results were challenged with molecular dynamic studies of 100 ns long simulation in triplicates (100 ns \times 3 = 300 ns) and were analyzed for RMSD, RMSE, RoG, H-bond number and distance, SASA, and secondary structure assessment performed together with principal component analysis and the free-energy landscape diagram, which indicated that the ChAT-A β complex system was stable throughout the simulation time period with no abrupt motion during the evolution of the simulation across the triplicates, which also validated the robustness of the simulation study. Finally, the free-energy landscape analysis confirmed the docking results and demonstrated that the ChAT-A β complexes were energetically stable despite the unstructured nature of C- and N-terminals in A β peptides. Overall, this study supports the reported in vitro findings that A β peptides, particularly A β_{42} , act as endogenous ChAT-Potentiating-Ligand (CPL), and thereby supports the hypothesis that one of the native biological functions of A β peptides is the regulation of acetylcholine homeostasis.

Keywords: β -amyloid; choline acetyltransferase; cholinergic system; Alzheimer's disease; in silico modeling



Citation: Baidya, A.T.; Kumar, A.; Kumar, R.; Darreh-Shori, T. Allosteric Binding Sites of A β Peptides on the Acetylcholine Synthesizing Enzyme ChAT as Deduced by In Silico Molecular Modeling. *Int. J. Mol. Sci.* **2022**, *23*, 6073. <https://doi.org/10.3390/ijms23116073>

Academic Editor: Maria Laura Giuffrida

Received: 8 April 2022

Accepted: 25 May 2022

Published: 28 May 2022

Publisher's Note: MDPI stays neutral with regard to jurisdictional claims in published maps and institutional affiliations.



Copyright: © 2022 by the authors. Licensee MDPI, Basel, Switzerland. This article is an open access article distributed under the terms and conditions of the Creative Commons Attribution (CC BY) license (<https://creativecommons.org/licenses/by/4.0/>).

1. Introduction

Alzheimer's disease (AD) is the most prevalent form of dementia affecting millions of people worldwide. It is characterized by the presence of pathological markers such as senile plaques and neurofibrillary tangles in the brain of AD patients. Senile plaques are mainly composed of aggregated Amyloid- β peptide (A β ; product of amyloid precursor protein (APP) cleavage) [1]. A β peptides can range from 36 to 43 amino acids depending on the enzyme cleavage sites, but the most common pathological forms are A β_{40} and A β_{42} [1,2]. A β_{42} is considered more toxic and highly prone to aggregation and accumulation as compared to A β_{40} . Another pathological feature, prominently found in AD brains, is cholinergic dysfunction that has been linked to cognitive decline and memory impairment in AD patients [3]. Indeed, loss of basal nuclei cholinergic neurons is shown to be directly associated with cognitive impairment in AD [4,5]. However, the exact cause of cholinergic

deficit and how it is related to other pathological changes in AD is still puzzling researchers around the world.

Cholinergic neurons, defined by the expression of the acetylcholine (ACh) synthesizing enzyme choline acetyltransferase (ChAT; EC 2.3.1.6), are projected from certain nuclei in the basal forebrain throughout the brain [6] and regulate key cognitive functions such as attention, memory, and learning. It has been shown that the cholinergic signaling machinery, including high-affinity choline transporter (hChT) and ChAT, is highly susceptible to A β peptides and its aggregated forms [4,7–9].

The innate physiological function of A β peptides is still unknown and the focus of the research community has been on the toxicity of these peptides and their aggregates. However, studies have shown that A β can act as a ligand of RAGE (receptor for advanced glycation end products) and regulate key inflammatory signaling pathways [10]. In addition, physiological concentrations of A β_{42} peptide can activate the MAPK (mitogen-activated protein kinase) cascade in the hippocampus via the $\alpha 7$ nicotinic acetylcholine receptor [11]. In mammals, MAPK cascade is involved in learning and memory formation [12]. Most importantly, recent studies have suggested a more prominent role of A β peptides in synaptic and extrasynaptic ACh homeostasis. We have previously shown that A β peptides interact with acetyl- and butyryl-cholinesterase (AChE and BChE) in an apolipoprotein facilitated manner, and thereby can modulate cholinergic signaling by forming highly stable and ultra-active soluble ACh-degrading complexes called BA β ACs [13].

Other studies have shown that short- and long-term exposure to A β peptides can lead to a reduced ACh synthesis and release from neuronal cell cultures as well as neurodegeneration and cognitive impairment in animal models [14–25]. However, it is not clear whether these effects are caused by a direct or an indirect mode of action of A β peptides on the activity of the core cholinergic enzyme ChAT. In contrast, we have shown that A β peptides, in particular A β_{42} , directly interact and allosterically enhance rather than reduce the catalytic rate of ChAT at physiological concentrations representative of A β levels in the CSF of AD patients and healthy controls (Figure 1) [26].

Given that cholinergic deficit is one of the key features in major dementia disorders, the findings that A β peptides can allosterically increase biosynthesis of ACh opens a new avenue for the development of a new class of cholinergic enhancing therapeutic strategy based on improving ACh biosynthesis that we are calling ChAT-Potentiating-Ligands (CPLs), as opposed to the cholinesterase inhibitors approach based on inhibiting the degradation of ACh by cholinesterases. In the primary paper of our study, we have reported that A β_{40} exhibited CPL activity with an EC₅₀ value of 800 pg/mL (or 185 pM) while A β_{42} peptides showed a 10-fold higher CPL potency as deduced by an EC₅₀ value of 68 pg/mL (or 15 pM) [26]. These EC₅₀ values are fully in the range of the expected concentration of A β peptides in the human brain, as deduced by the known concentration of A β peptides in human cerebrospinal fluid. Thereby, it is imperative to determine the molecular fingerprint of the interaction between ChAT and the A β peptides as the only known endogenous CPL.

Therefore, the current study had two main objectives. Firstly, we aimed to shed further light on the physiological role of A β peptides in ACh regulation, and secondly, to investigate and elucidate the molecular fingerprint of the binding mechanism of A β peptides on ChAT governing the CPL activity of the A β peptides, using advanced *in silico* molecular docking and molecular dynamics studies. We report here the results of both the docking and 100 ns molecular simulation analyses in terms of the molecular dynamic parameters, such as root mean square deviation (RMSD), radius of gyration (Rg), root mean structure fluctuation (RMSF) and H-bond functionality values. We show that these analyses indicate that A β peptides can physically interact with ChAT protein, forming highly stable ChAT-A β complexes as deduced by a free-energy landscape analysis. In addition, we provide details on the stability and robustness of the ChAT-A β peptides simulated system.

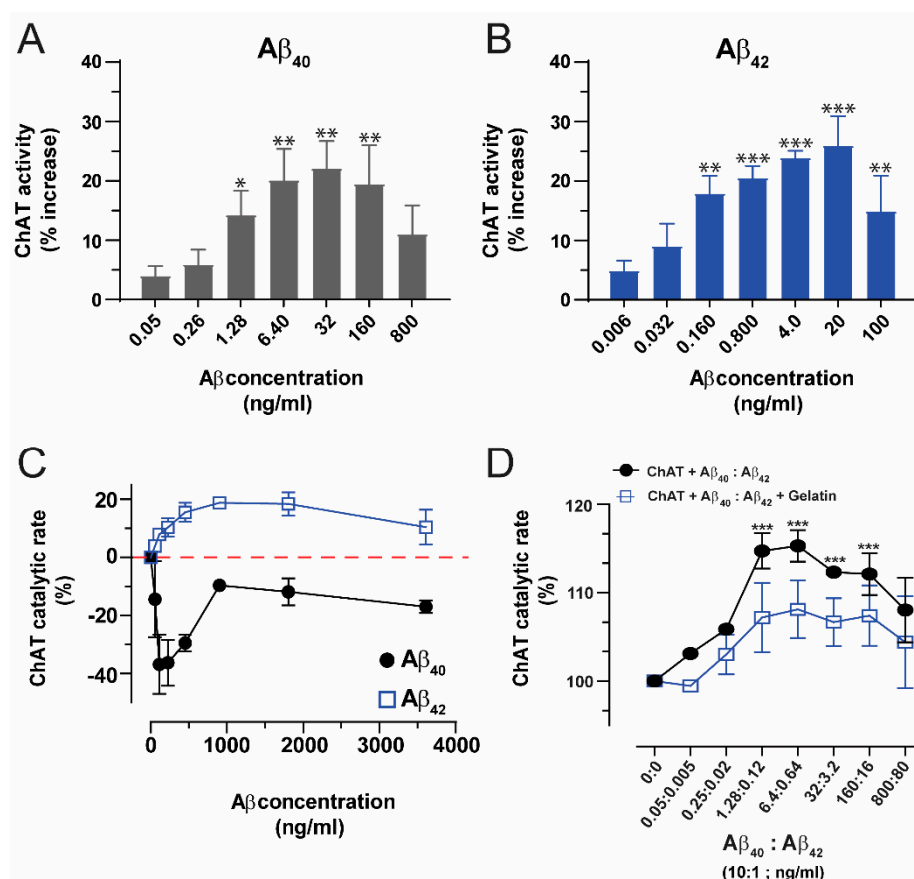


Figure 1. Soluble A β peptides specifically and allosterically activate ChAT at physiological concentrations via direct interaction (adapted and reproduced from Kumar et al. [26], under the terms of the CC BY license). ChAT was incubated with A β peptides at physiological concentration ranges and changes in its activity were monitored using the kinetic ChAT fluorometric assay. (A) The percent changes in the rate of ChAT (Δ RFU/hr) by A β_{40} at the specified concentration range of 0 to 800 ng/mL (B) The corresponding percent of changes in ChAT activity by A β_{42} , at the specified concentration range of 0 to 100 ng/mL. The activity of the control sample (ChAT with no A β) was considered as 100% to calculate the percentage increase in ChAT activity in the presence of different A β concentrations. The values are shown as mean \pm SEM of ≥ 3 independent experiments. (C) The effect of high concentrations (non-physiological range) of A β peptides on ChAT activity was also monitored. ChAT was incubated with different concentrations of A β_{40} and A β_{42} peptides, ranging from 0 to 3800 ng/mL in 96-well plates. The values are shown as mean \pm SEM of two independent experiments. For A β_{40} (A), the symbols * and ** represents p -values < 0.005 and < 0.0003 , respectively, relative to the control (no A β_{42}). The comparisons are based on one-way ANOVA analysis and Fisher's LSD post-hoc test. (D) Both A β_{40} and A β_{42} are present simultaneously in biological fluids at a 10:1 ratio. Therefore, we measured ChAT activity in the presence of various concentrations of mixtures of A β peptides to somewhat mimic the in vivo conditions. Graph shows the percent changes in ChAT activity at the specified A β mixture concentrations with or without gelatin (which mimics a high protein concentration microenvironment, as expected physiologically in biological fluids). The activity of the control sample (ChAT with no A β) was considered 100%. The values are shown as mean \pm SEM of ≥ 2 independent experiments. *** $p < 0.0001$, relative to the control (no A β), based on one-way ANOVA analysis and Fisher's LSD post-hoc test.

2. Results

Amyloid- β and its exact native function are still questions of debate among researchers worldwide. In our recently published paper, we have shown that A β peptides can upregulate the activity of the core-cholinergic enzyme ChAT by direct interaction at physiological concentration ranges and this enhanced catalytic efficiency was persistent even at the

physiological ratio of A β ₄₀:A β ₄₂ mixture (Figure 1; adapted and reproduced from Kumar et al. [26], under the terms of the CC BY license). Here, molecular docking studies were performed using a Cluspro protein-protein docking web server to elucidate the possible interaction mechanism of A β peptides with ChAT. The final protein-protein docking cluster analysis identified 29 clusters for ChAT-A β ₄₀ and ChAT-A β ₄₂ complexes. The most probable binding cluster for ChAT-A β ₄₀ complex Cluster-0 with a maximum of 88 members and the lowest energy (−989.5 kcal/mol). The corresponding was Cluster-0 for ChAT-A β ₄₂ complex had the maximum members of 134 and the lowest energy of −999.6 kcal/mol (Table 1).

Table 1. Probabilistic binding clusters of A β ₄₀ and A β ₄₂ on ChAT.

Cluster	Representative Complex	ChAT-A β ₄₀		ChAT-A β ₄₂	
		Cluster Size	Weighted Score (Balanced)	Cluster Size	Weighted Score (Balanced)
0	Center	88	−920.6	134	−973.8
	Lowest Energy	88	−989.5	134	−999.6
1	Center	75	−850.2	94	−926.2
	Lowest Energy	75	−1011.0	94	−1111.3
2	Center	51	−966.0	84	−884.8
	Lowest Energy	51	−966.0	84	−991.3
3	Center	46	−878.0	66	−851.2
	Lowest Energy	46	−975.8	66	−875.5
4	Center	45	−826.8	51	−858.4
	Lowest Energy	45	−905.4	51	−858.4
5	Center	41	−909.3	46	−851.0
	Lowest Energy	41	−951.7	46	−851.0
6	Center	38	−815.5	23	−883.5
	Lowest Energy	38	−936.2	23	−883.5
7	Center	36	−824.2	22	−911.2
	Lowest Energy	36	−905.1	22	−911.2
8	Center	35	−976.1	20	−822.4
	Lowest Energy	35	−976.1	20	−888.7
9	Center	34	−928.1	20	−920.8
	Lowest Energy	34	−949.1	20	−920.8
10	Center	27	−833.2	18	−813.1
	Lowest Energy	27	−920.9	18	−932.6

ChAT = choline acetyltransferase, A β = Amyloid- β peptide.

The predicted models were well justified based on the scores, as it implies the linear combinations of several energy terms, such as the attractive and repulsive van der Waals energy describing the complementary shape, and one or more terms denoting the electrostatic binding energy and cluster sizes. The 3D cartoon representations for the top three clusters of ChAT-A β ₄₀ are given in (Figure 2B–D). The putative entrances of the catalytic tunnel on ChAT are indicated by a *red circle* (for choline/ACh entrance site) and *yellow circle* (for ACoA/-CoA entrance site; Figure 2). Intriguingly, in the cluster-1, A β ₄₀ seemed to completely cover the mouth of the choline/ACh entrance site of ChAT's catalytic tunnel (*red circle* in Figure 2C), whereas the most probable cluster-0 indicated that A β ₄₀ nearly touched the ACoA/-CoA entrance site on ChAT (*yellow circle* in Figure 2B) as well as the cluster-2 indicating that the A β ₄₀ covers the mouth of ACoA/-CoA entrance site on ChAT (*yellow circle* in Figure 2D). Thus, these binding cluster analyses intuitively suggest that the A β ₄₀ binding at cluster-1, but not the cluster-0 or -2, could block the influx of the substrate, choline or ACh, and thereby the access of the enzyme to these substrates. Importantly,

this could explain why in some of our in vitro experiments, the A β_{40} either inhibited or induced minimal activation of ChAT (Figure 1C) [26].

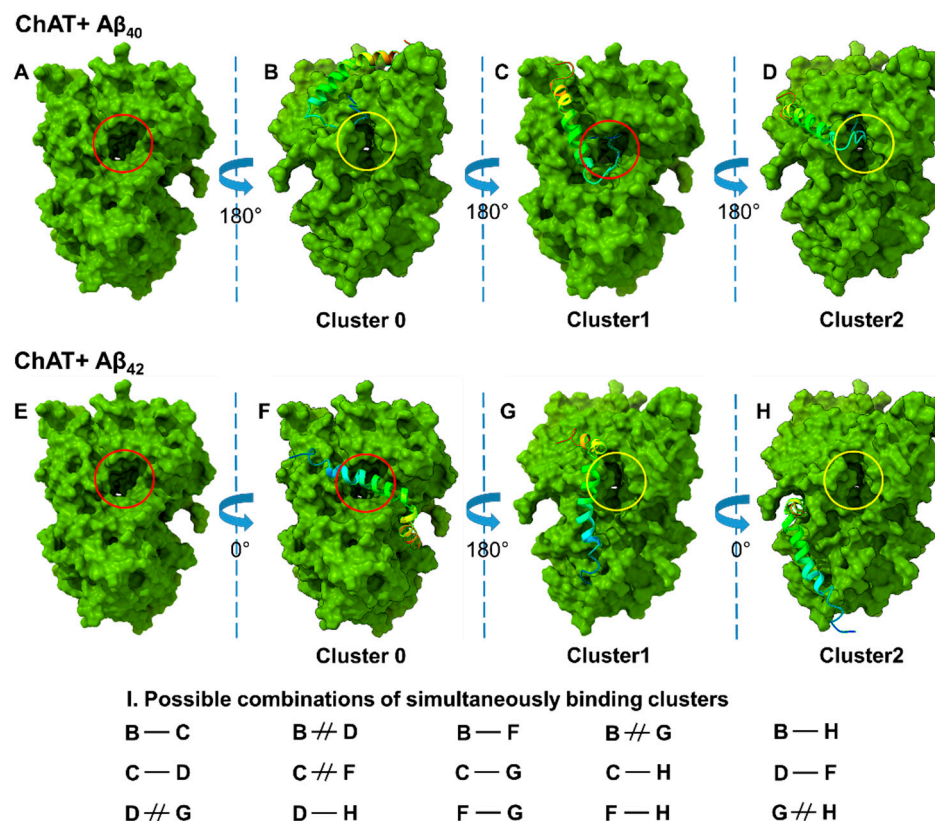


Figure 2. In silico molecular docking analyses reveal the potential binding sites for A β peptides on ChAT. Molecular docking for ChAT and A β peptides was performed using Cluspro web server as described in the method section. (A,E) show the 3D representation of ChAT protein, where the choline-entrance of the catalytic tunnel is indicated by *red circle*. (B–D) show the most probable binding-sites for clusters-0, -1 and -2 of A β_{40} peptides, respectively. The *yellow circle* highlights the Acetyl-CoA-entrance of the catalytic tunnel. A comparison of (B–D) indicates that the binding of A β_{40} at cluster-1, but not cluster-0 or -2, will most likely block the entrance of choline into the catalytic tunnel of ChAT, whereas A β_{40} binding in cluster-2 will interfere with the Acetyl-CoA-entrance site. (F–H) illustrate the most probable binding-site clusters -0, -1, and -2 for A β_{42} peptide, respectively. Similar to A β_{40} , one out of the top three clusters of A β_{42} (cluster-0) also overlaps the choline-entrance site of the catalytic tunnel (F). Theoretically, it is possible that two A β peptides can simultaneously bind to one ChAT molecule. The table (I) shows all such possible/excluding combinations. For example, the cluster-0 (B) will most likely exclude simultaneous binding of another peptide at cluster-2 (D) or vice versa. This is denoted as B \neq D. In contrast, it is possible for two A β_{42} peptides to bind simultaneously to ChAT, namely at cluster -0 and -1 (F–G), or at cluster-0 and -2 (F–H).

For ChAT-A β_{42} complex, the top three clusters are presented as a 3D cartoon in (Figure 2F–H), illustrating the most probable binding sites of A β_{42} on ChAT. Again, the position of the choline/ACh entrance site of the catalytic tunnel is highlighted by a *red circle* (in Figure 2E).

Surprisingly, like A β_{40} , A β_{42} appeared to completely overlap the catalytic tunnel, but in this case it was in the most probable cluster-0 (Figure 2F), and not in the cluster-1 like A β_{40} . Nonetheless, there are two additional binding sites for A β_{42} that are in close vicinity of the mouth of the ACoA/-CoA entrance site on the catalytic tunnel, namely the clusters -1 and -2 (*yellow circle*; Figure 2G,H). These sites might best explain the improved catalytic efficiency of ChAT by A β_{42} peptides (compare Figure 1A,B). In addition, we have compiled the simultaneous possible bindings for A β_{42} and A β_{40} as depicted in (Figure 2I).

For instance, binding of A β ₄₂ at cluster-1 (Figure 2G) will most likely exclude binding of A β ₄₀ at cluster-0 (Figure 2B) or vice versa. In contrast, it is also possible that two A β bind simultaneously on a ChAT molecule, e.g., conditions C-H or F-H in (Figure 2I).

Next, the predictions of the binding mode of A β peptides to ChAT by the docking analyses were challenged with advanced molecular dynamic (MD) simulation analysis in order to realize the conformational changes and stability during the course of interaction. The time required for the biological phenomenon to occur is considered as the optimum time for simulation. Based on the resources available, the calculations were tuned and, keeping our objective in mind to fulfil the criteria that the RMSD stabilizes over the period of time, were indicated by a stable line that concludes that the system has reached convergence and is comparatively stable. To explore the global minima in the energy landscape, the MD trajectories were run and analyzed under physiological environment for a 100 ns-long simulation time period in triplicates. The results of the molecular dynamic analysis of the first primary run are shown in (Figure 3) as a measure of the stability and quality of the simulated system. The RMSD plot suggested that the ChAT protein remained stable from 0.1–0.28 nm, as shown in (Figure 3A). The averages of the triplicates were plotted, as represented in Supplementary Figure S1. The results are well within the limits with low uncertainties, which are denoted as the 'Y' bar error (standard deviation) obtained from three independent 100 ns simulations. The RMSD value of A β peptides for the first run (Figure 3B) seems to be in the ranges of 0.3–1.73 nm, which indicates their stability in the complex system throughout the simulation time. Likewise, the averages obtained from the triplicate runs were plotted, as shown in Supplementary Figure S2. The standard deviation is larger compared to the protein structure, which is due to the flexibility of the peptide as it interacts with the protein surface throughout the course of simulation. The radius of gyration (RoG) of the complex was also determined, as shown in (Figure 3C), to further understand the compactness and overall dimensions of the protein structure. The RoG values for the first run were in line with the RMSD values as well as stable and relatively low ranging between 2.5 and 2.65 nm for the ChAT-A β complex. This indicated that the formed complex retained a compact folded conformation throughout the simulation time. The individual RoG plots for all three runs of the ChAT-A β complex clusters are shown in Supplementary Figure S3. The results from the triplicates indicate that the RoG values remained stable with relatively low variation that were in an acceptable range.

Furthermore, to understand the dynamic behaviors of the amino acid residues and flexibility of the protein structure during the interaction period of the simulation, we recorded and analyzed the root mean square fluctuation (RMSF) as a measure of individual amino acid fluctuation throughout the course of simulation. The magnitude of individual amino acid residual flexibility is represented by the corresponding height of the peaks. RMSF plots of ChAT protein for the first run indicate no major fluctuation in the ChAT core structure (Figure 3D), with a value of 0.05–0.4 nm for the amino acid residues. However, the C- and N-terminals of the ChAT protein exhibited higher structural flexibility with values ranging up to 0.7 nm. This is expected since they are naturally exposed to solvent surface. The average RMSF values of the ChAT protein, along with the standard deviation for the three runs are shown in Supplementary Figure S4, which shows low fluctuations. Likewise, the RMSF value of the A β peptides (Figure 3E) was observed between the acceptable limits of 0.1–1.2 nm indicating the relative stability of the A β peptides in the system. The C- and N-terminal of A β showed higher RMSF value, indicating the higher flexibility of the regions due to the unstructured nature, as reported based on NMR structural studies [27,28]. The average RMSF values of the A β peptides, along with the standard deviation for the three runs is shown in Supplementary Figure S5. The larger variation most likely reflects the higher flexibility of the C- and N-terminal of A β peptides. Overall, the RMSF suggested that A β was tightly bound with the ChAT protein, despite these C- and N-terminal flexibilities and the overall ChAT-A β complexes remained stable for the whole simulated time.

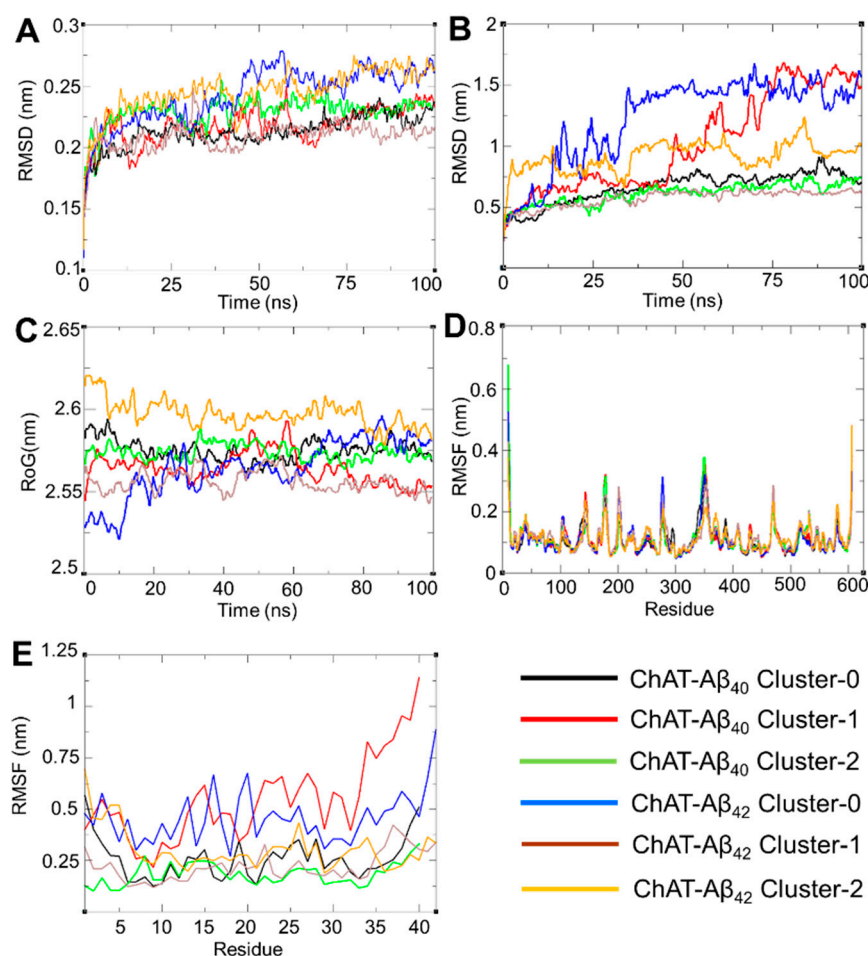


Figure 3. Molecular dynamics simulation analyses support the potential interaction and stability between A β peptides and ChAT. (A) represents root mean squared deviation (RMSD) plots as a function of simulation period for the ChAT protein. (B) shows the root mean squared deviation (RMSD) plots for A β peptides. (C) illustrates the radius of gyration (RoG) plots for the complexes. (D,E) show root mean squared fluctuation (RMSF) for ChAT and A β amino acid residues, respectively. The clusters are represented by the given color scheme. All of the graphs were plotted with the QtGrace software package.

Hydrogen bonding plays a central role during the interactions, formation and stabilization of protein complexes. The typical distance criterion for a hydrogen bond donor and acceptor atoms is $\leq 3.5 \text{ \AA}$ (0.35 nm) with an angle of $180^\circ \pm 30^\circ$ between hydrogen bond donor and acceptor. Therefore, we also calculated the average number of hydrogen bonds formed during ChAT-A β peptide interactions throughout the 100 ns simulation with a cut-off value of 0.35 nm, as shown for the first run in Figure 4A. The individual landscapes for the hydrogen bonds formed between ChAT-A β peptides during all the three runs is shown in Supplementary Figure S6. The results were consistent with respect to each other, which indicates that a stable number of hydrogen bonds were maintained throughout the simulation period. The average hydrogen bond distance was also calculated, which was found to be about 0.3 nm, which is within the expected range (Figure 4B). The results from all the triplicates were very similar (Supplementary Figure S7), with an average hydrogen bond distance of about 0.3 nm.

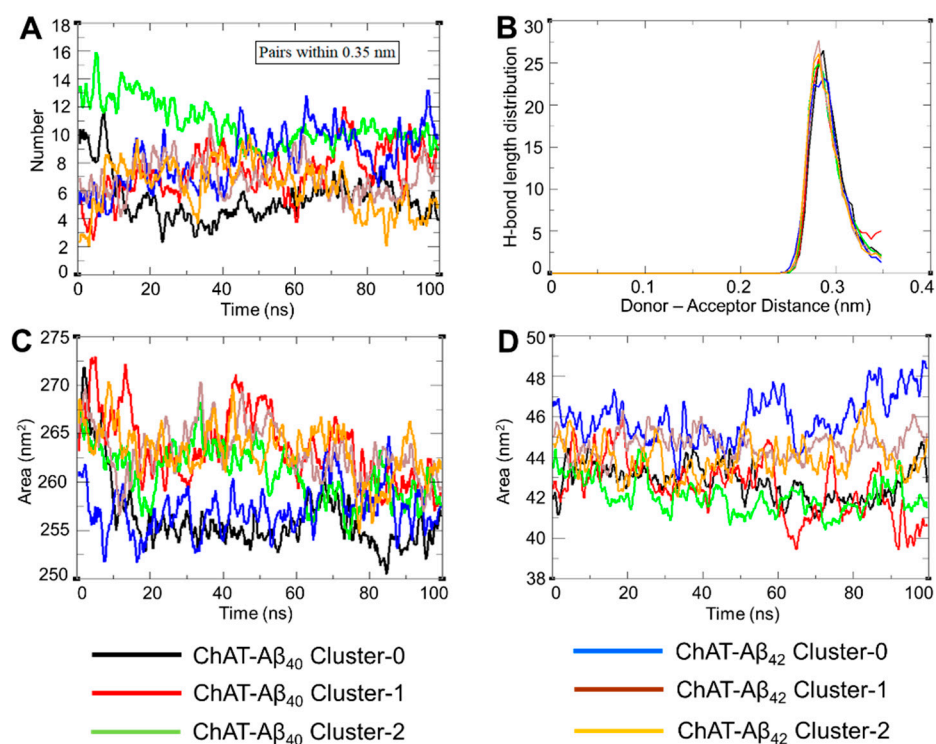


Figure 4. The ChAT-A β complex formation and stabilization based on hydrogen bonding landscape analysis. H-bonding plays a central role during protein interactions; thereby (A) shows the average number of hydrogen bonds formed between ChAT-A β peptides during 100 ns simulation trajectory. (B) illustrates the average hydrogen-bond distance around the cut-off for donor-acceptor distance that was set at 0.35 nm. (C,D) denote the change in total solvent accessible surface area (SASA) of the ChAT protein and the total solvent accessible surface area of the A β peptides, respectively, corresponding to the simulation time-period of the complex system. The clusters are represented by the given color scheme.

Moreover, we performed a solvent accessible surface area (SASA) analysis, which measures the surface area of the biomolecule accessible by the solvent (biofluids), and helps in predicting the stability of the hydrophobic core of the protein. These hydrophobic contacts are crucial indicators of the compactness of the tertiary structures of a protein [29]. We found that the SASA profile of each ChAT-A β cluster complex is consistent with its radius of gyration as there was a slight decrease in SASA. This in turn indicates a contracted conformation of the complex, as a higher SASA profile reflects a relative expansion of the protein surface area and would have resulted in a more fluctuating radius of gyration. The values ranged from 250–275 nm² for ChAT proteins (Figure 4C) and 39–49 nm² for A β peptides (Figure 4D) for the first run. The averages from the triplicates along with their standard deviation is shown in Supplementary Figures S8 and S9. The results were consistent with reasonably low variations in the reproduction of the SASA profiles. Furthermore, SASA for the ChAT protein seemed to be reduced at the end of the simulation (Figure 4C), indicating that the A β peptides are interacting with the ChAT protein and are causing changes in the structure and surface residues of the ChAT protein in such a way that it further shields its hydrophobic core accessible to the solvent. Whilst for the A β peptides, SASA showed an increase towards the end of the simulation with constant changes due to the interaction with ChAT protein.

To unravel the connection between the internal motion and the secondary structures, such as the coil, beta sheets, beta-bridge, bend, turn, and helices throughout the simulation time, a Dictionary of Secondary Structure of Protein (DSSP) analysis was instigated, which identifies protein sheets and helix assignments solely on the basis of backbone-backbone hydrogen bonds. We performed TESSE (time-evolution of the secondary structural elements)

analyses for ChAT and A β peptides, which are visually summarized in Supplementary Figures S10 and S11, respectively. The analyses in (Figure S10) further reveal that the ChAT protein maintained its secondary structure throughout the simulation period without much conformational change, since all the amino acid residues maintained their structure during the simulation period.

Moreover, we observed that the ChAT protein retained a greater number of alpha helices, which is about 40% of the amino acids remained in this state, as compared to coils, beta sheet, turn, bend, 5-helices, and 3-helices. This observation is based on data presented in Tables 2 and 3, which show the percentage of secondary structure distribution in the trajectory clusters for A β_{40} and A β_{42} on ChAT in each cluster system, respectively. The occurrence and maintenance of alpha helices is the most stable dominant structural element. This was a common feature of protein secondary structure in the ChAT protein throughout the simulation period, reflecting its compactness, energetically most favorable conformations, and slow steady change throughout the simulation. On the other hand, the A β peptides seemed to be constantly changing over the simulation time period, as is evident by containing a greater number of turns and random coils (Figure S11), which could reflect an interplay with the ChAT catalytic mouth of Choline/ACh entrance site.

Table 2. Average secondary structure across the trajectory clusters of A β_{40} on ChAT.

% Secondary Structure	ChAT-A β_{40} Cluster-0		ChAT-A β_{40} Cluster-1		ChAT-A β_{40} Cluster-2	
	ChAT	A β_{40}	ChAT	A β_{40}	ChAT	A β_{40}
Coil	21	26	22	34	21	30
Beta sheet	14	0	14	0	15	0
Beta bridge	0	0	1	0	0	0
Bend	10	13	10	17	9	14
Turn	11	32	11	20	11	18
A-helix	40	20	40	17	40	25
5-helix and 3-helix	4	10	3	12	3	13

Table 3. Average secondary structure across the trajectory clusters of A β_{42} on ChAT.

% Secondary Structure	ChAT-A β_{42} Cluster-0		ChAT-A β_{42} Cluster-1		ChAT-A β_{42} Cluster-2	
	ChAT	A β_{42}	ChAT	A β_{42}	ChAT	A β_{42}
Coil	21	21	21	18	22	21
Beta sheet	14	0	14	0	14	0
Beta bridge	1	0	1	0	0	0
Bend	10	14	10	8	10	11
Turn	11	32	12	24	10	26
A-helix	40	21	40	42	41	23
5-helix and 3-helix	3	13	2	7	3	19

We did a Principal Component Analysis (PCA), also known as essential dynamics based on the principles of covariance matrix, to identify the most important conformational degrees of freedom of the simulation system. It helps in shortening the large dimensions of the data set to the major principal components that represents the considerable variations that can sufficiently explain the overall motions of the protein. The eigenvalues for the complex are shown in (Figure 5), where it is clearly evident that the first four components explain the most variation in the data which is 53.58, 78.71, and 52.70 for cluster-0, -1, and

-2 of $A\beta_{40}$ peptides, respectively, and in case of $A\beta_{42}$ peptides it is about 72.85, 49.25, and 52.43 for the cluster-0, -1, and -2, respectively. The plot shows that the eigenvalues after the fourth principal component starts to make a straight horizontal line. Thus, we have selected the first two principal components to plot our essential dynamics plot.

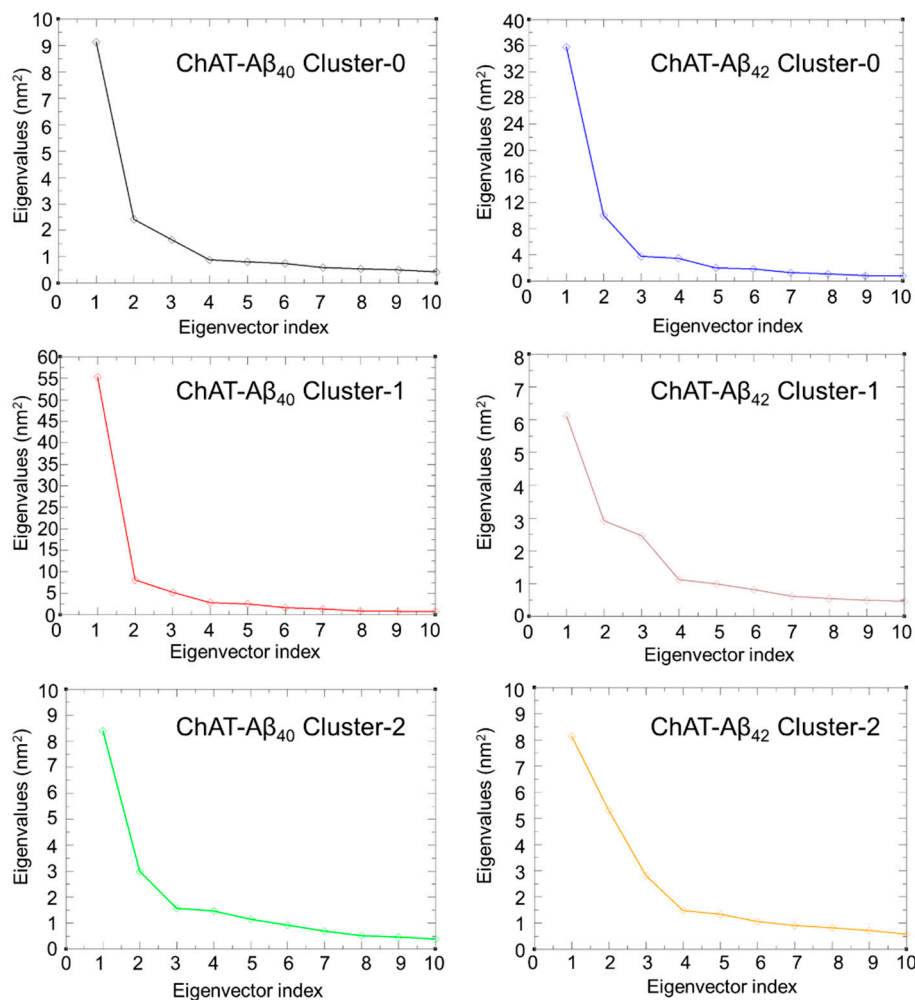


Figure 5. This represents the eigenvalues of each principal component for all the ChAT- $A\beta$ peptides complex simulated systems. Principal component (PC) analysis tries to find combinations of features that leads to the maximum separation between the data points. The analysis suggests that the first three PC eigenvector accounts for most of the motions in the system, while from the fourth PC eigenvector the contribution become less important. We used the first two PCs to generate the cluster projections by plotting it on x and y axis, respectively, to explain the data points.

The plotted 2D graph for the first two principal components (Figure 6), represents the various conformations taken by the protein in the course of simulated period. The changes in the ChAT- $A\beta$ complex system indicates that $A\beta$ peptides affected the flexibility of the ChAT protein. ChAT- $A\beta_{40}$ cluster-0 and -2 and ChAT- $A\beta_{42}$ cluster-1 and -2 complexes demonstrated concentrated conformational sampling, indicating a stable state conformation occupied by the overall system. While the ChAT- $A\beta_{40}$ cluster-1 and the ChAT- $A\beta_{42}$ cluster-0 display a widespread distribution of the conformational space, this can be due to larger conformational changes in the protein structure, thus indicating that a wide range of conformational states are occupied by the complex over the simulation time.

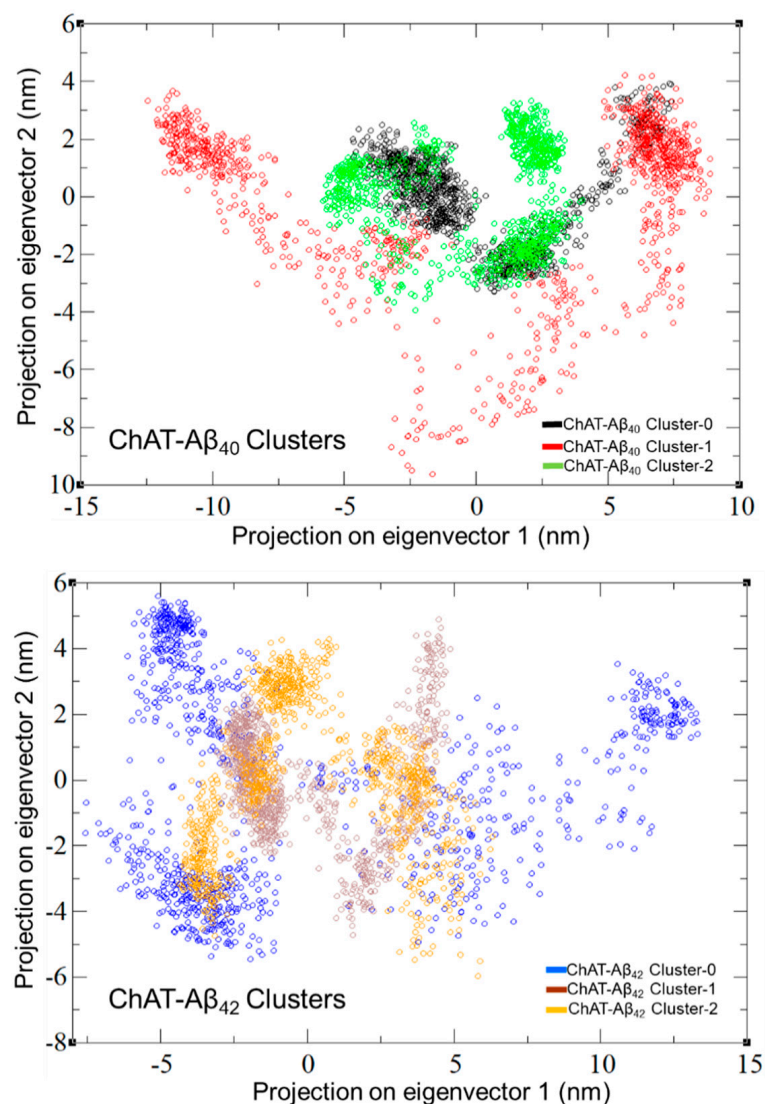


Figure 6. Representation of the projection of the first two principal components for the ChAT-A β complex system. Each dots represent a specific conformational state of the ChAT protein in the complex system with A β . Congregated clusters of the dots indicate that the protein did not go through any major conformational changes, whereas the widespread dots indicate more flexibility of the protein in the complex and, hence, some major conformational changes that might take place. Overall, the graphs illustrate the close concentrated distribution of the conformational sampling for the majority of the ChAT-A β complexes clusters except for the ChAT-A β_{40} cluster-1 and ChAT-A β_{42} cluster-0, which exhibit widespread distribution of conformational sampling.

Free-energy landscape (FEL) is a representation of possible conformations taken by a protein in molecular dynamics simulation along with the Gibbs free energy. FEL represents two variables that reflect specific properties of the system and measure conformational variability. To visualize the energy minima landscape of bound ChAT-A β complex, we studied the free-energy landscape (FEL) against radius of gyration (RoG) and root-mean-square deviation (RMSD) as the two reaction coordinates. This revealed the changes in the Gibbs free energy (ΔG) values between 0 and 9.950 kJ/mol for A β_{40} (Figure 7) and from 0 to 10 kJ/mol for A β_{42} (Figure 8) complexes.

The shape and size of the minimal energy area (shown in blue) indicate the stability of the ChAT-A β complex system. Smaller and more centralized blue areas represent the complex within the cluster with the highest stability. The narrow funnel formed as seen in the 3D projections show the dynamic of the change in conformation with the time of simulation required to attain a native structure with least energy. Overall, the 3D plots illustrate that the overall complexes formed a single funnel, which together with the 2D contour plot clearly indicates the complexes having one local energy minima, and hence reflecting a stable folding process in the system.

Thereafter, we used the insights from the free-energy landscape analysis and constructed the energy minima structures (Figure 9). These structures were in good agreement with those constructed through molecular docking analysis, reinforcing the insight about the potentially stable binding sites for A β peptides on ChAT protein.

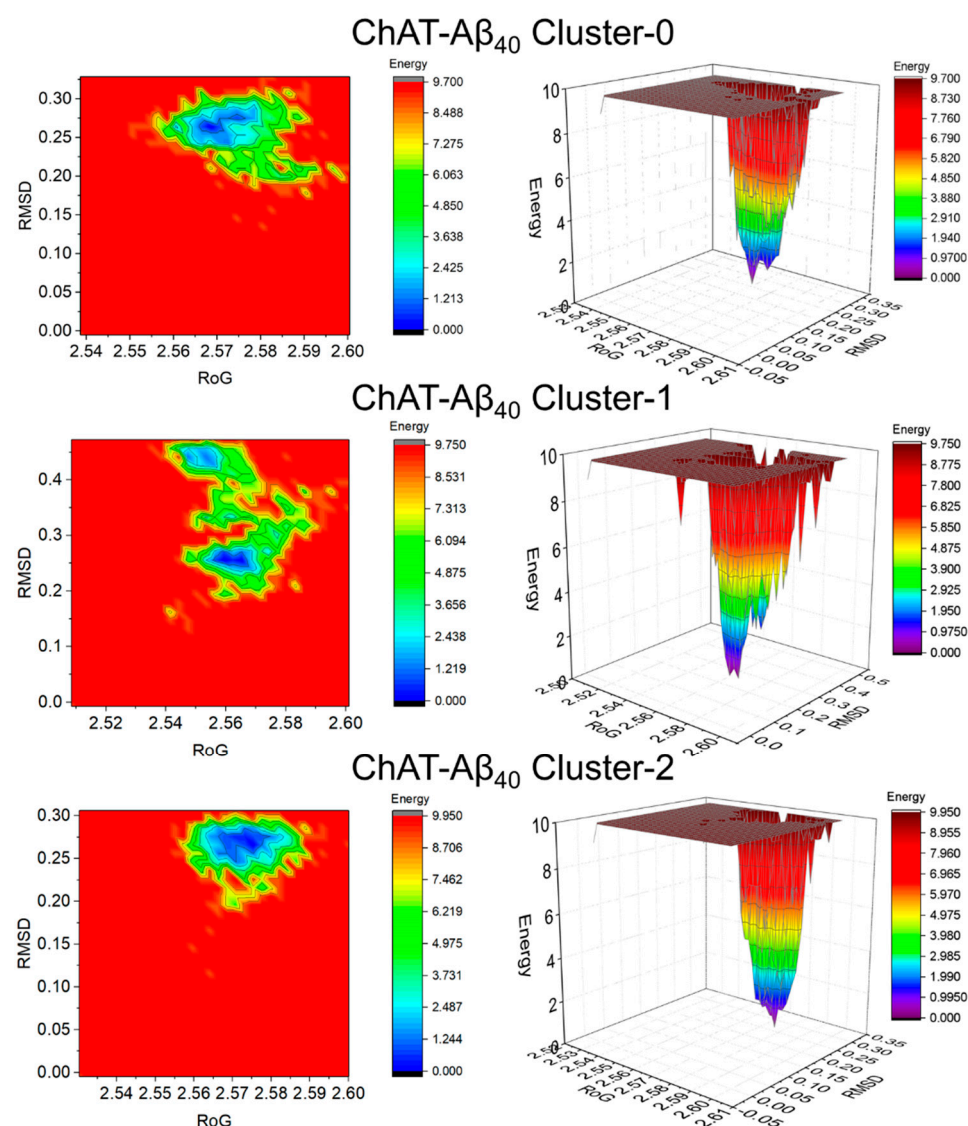


Figure 7. The 2D and 3D free-energy landscape diagrams as a function of RMSD and RoG as the two reaction coordinates of ChAT-A β_{40} clusters. The free energy is given in kJ/mol and indicated by color. The folding funnel of the complex system into a single narrow funnel indicate a stable folding process. The 2D contour plots and the 3D projections were plotted using OriginPro 2017 software (OriginLab Inc., Northampton, MA, USA). RMSD: Root mean square deviation, RoG: Radius of gyration.

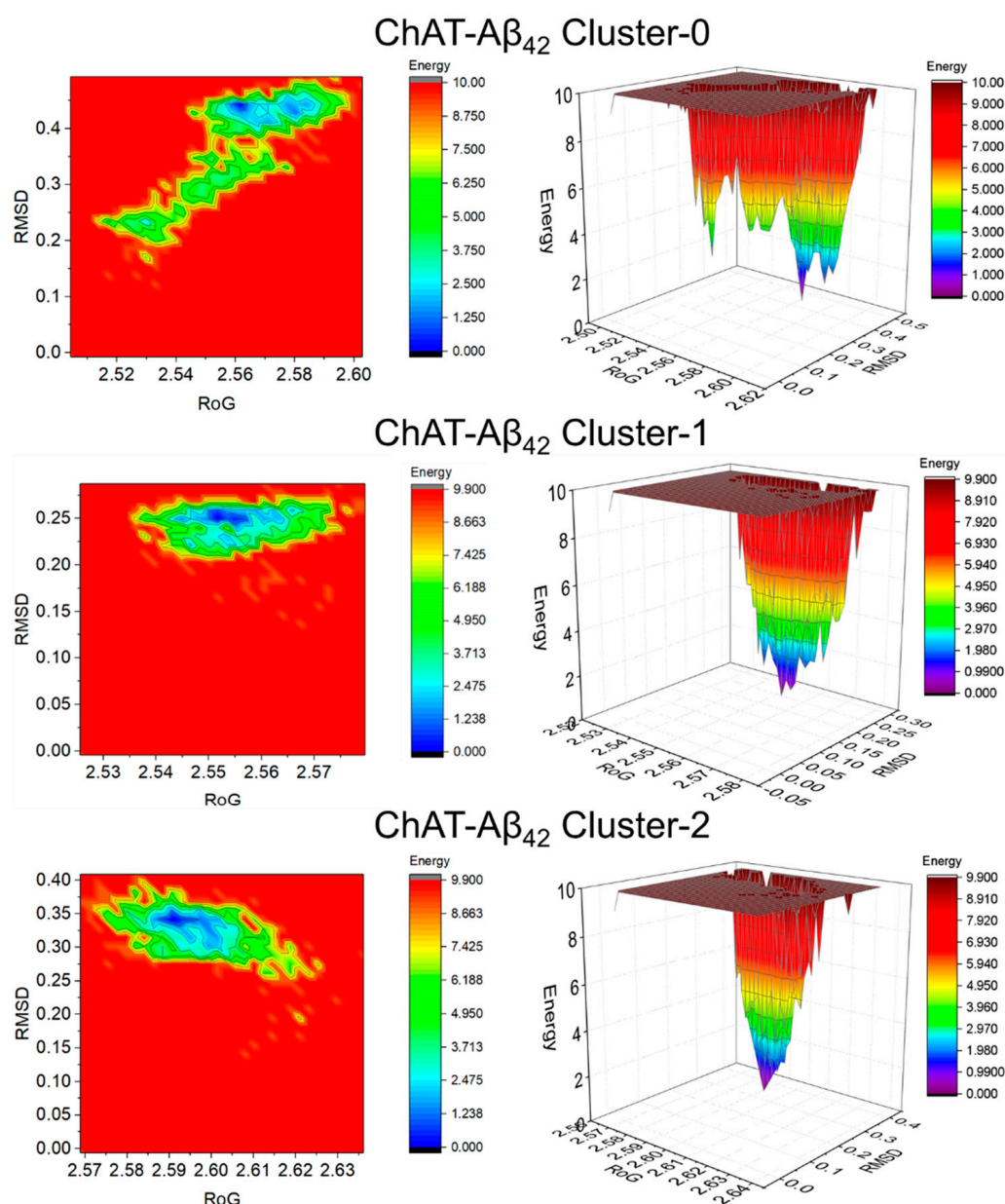


Figure 8. The 2D and 3D free-energy landscape diagrams as a function of RMSD and RoG as the two reaction coordinates of ChAT-A β_{42} clusters. The folding funnel of the complex system forms a single narrow funnel which indicates a stable folding process. The 2D contour plots and the 3D projections were plotted using OriginPro 2017 software (OriginLab Inc., Northampton, MA, USA). The free energy is given in kJ/mol and indicated by color. RMSD: Root mean square deviation, RoG: Radius of gyration.

The 3D cartoon representations for the top three clusters of ChAT-A β_{40} are given in (Figure 9K–M). The putative entrances of the catalytic tunnel on ChAT are indicated by a *red circle* (for choline/ACh entrance site; Figure 9J) and a *yellow circle* (for ACoA/-CoA entrance site; Figure 9). Intriguingly, in the cluster-1 (A β_{40} from the energy minima conformations) it can be appreciated that the complex seems to stabilize in a way that the N-terminal of the A β_{40} tends to hinder the opening of the choline/ACh entrance site of ChAT's catalytic tunnel (*red circle* in Figure 9L), whereas the most probable cluster-0 indicated that A β_{40} completely covered the ACoA/-CoA entrance site on ChAT (*yellow circle* in Figure 9K) as well as the cluster-2 indicating that the A β_{40} covers the mouth of ACoA/-CoA entrance site on ChAT (*yellow circle* in Figure 9M). Thus, these binding clusters analyses intuitively

suggest that the $A\beta_{40}$ binding at cluster-1 but not the cluster-0 or -2 could block the influx of the substrate, choline or ACh, and thereby the access of the enzyme to these substrates.

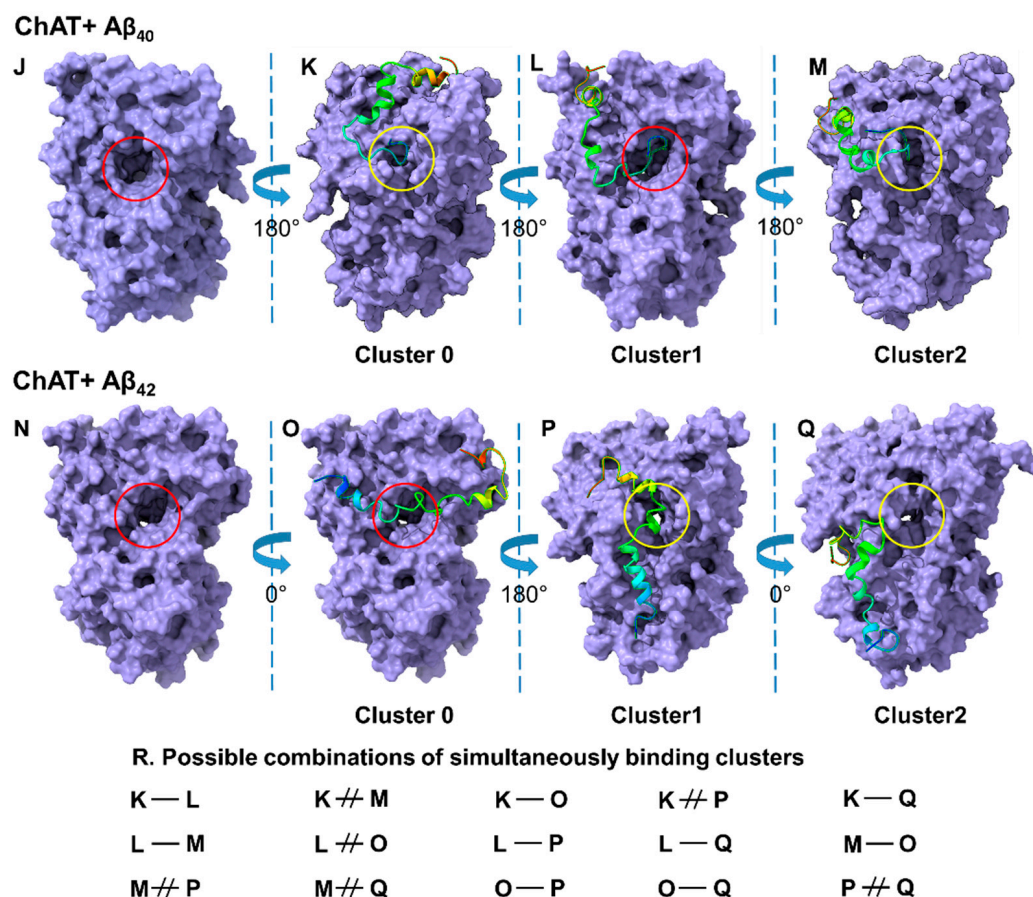


Figure 9. The most stable energy minima conformers of ChAT- $A\beta$ complexes. The outlined structures represent the Lowest Energy Minima conformers, i.e., the energetically favored complexes, constructed based on the free-energy landscape analysis as a function of root mean square deviation (RMSD) and radius of gyration (RoG) of ChAT- $A\beta$ clusters. (J,N) show the 3D representation of ChAT protein, where the choline entrance of the catalytic tunnel is indicated by a *red circle*. (K–M) show the Lowest Energy Minima conformers of the most probable binding-site clusters-0, -1 and -2 of $A\beta_{40}$ peptides, respectively. The *yellow circle* highlights the Acetyl-CoA-entrance of the catalytic tunnel. A comparison of (K–M) indicates that the binding of $A\beta_{40}$ at cluster-1, but not cluster-0 or -2, will most likely block the entrance of choline into the catalytic tunnel of ChAT. (O–Q) illustrate the Lowest Energy Minima conformers of the most probable binding-site clusters-0, -1, and -2 for $A\beta_{42}$ peptide, respectively. Similar to $A\beta_{40}$, one out of the top three clusters of $A\beta_{42}$ (cluster-0) also overlaps the choline-entrance site of the catalytic tunnel (O). The table (R) shows all possible/excluding combinations if two $A\beta$ peptides bind to one ChAT molecule simultaneously. For example, the cluster-0 (K) will most likely exclude simultaneous binding of another peptide at cluster-2 (M) or vice versa. This is denoted as $K \neq M$. In contrast, it is possible for two $A\beta_{42}$ peptides to bind simultaneously to ChAT, namely at cluster -0 and -1 (O,P), or at cluster-0 and -2 (O–Q).

For ChAT- $A\beta_{42}$ complex, the top three clusters are presented as a 3D cartoon in Figure 9O–Q, illustrating the most probable binding sites of $A\beta_{42}$ on ChAT. Again, the position of the choline/ACh entrance site of the catalytic tunnel is highlighted by a *red circle* (in Figure 9N). The most probable cluster-0 (Figure 9O) of $A\beta_{42}$ appeared to completely overlap the catalytic tunnel. Nonetheless, there are two additional binding sites for $A\beta_{42}$, namely the clusters-1 and -2 (*yellow circle*; Figure 9P,Q) that completely block and are in close vicinity of the mouth of the ACoA/-CoA entrance site on the catalytic tunnel, respectively.

In addition, we have compiled the simultaneous possible bindings for $A\beta_{42}$ and $A\beta_{40}$ as depicted in (Figure 9R). For instance, binding of $A\beta_{42}$ at cluster-1 (Figure 9P) will most likely exclude binding of $A\beta_{40}$ at cluster-0 (Figure 9K), or vice versa. In contrast, it is also possible that two $A\beta$ bind simultaneously on a ChAT molecule, e.g., conditions L-Q or O-Q in (Figure 9R). The final conformations obtained at the end of the simulation of the ChAT- $A\beta$ complexes are depicted in Supplementary Figure S12. These were resembling the lowest energy conformations (shown in Figure 9) indicating that towards the end of the simulation period, the ChAT- $A\beta$ complexes stabilized into a low energy conformation.

Furthermore, we have generated the contacts map for the ChAT- $A\beta$ complexes (Figures 10 and 11). It shows the amino acid residues of the ChAT protein that make a close contact with the $A\beta$ peptides. This can give hints about the necessary residues that are more likely to be interacting with each other during the complex formation.

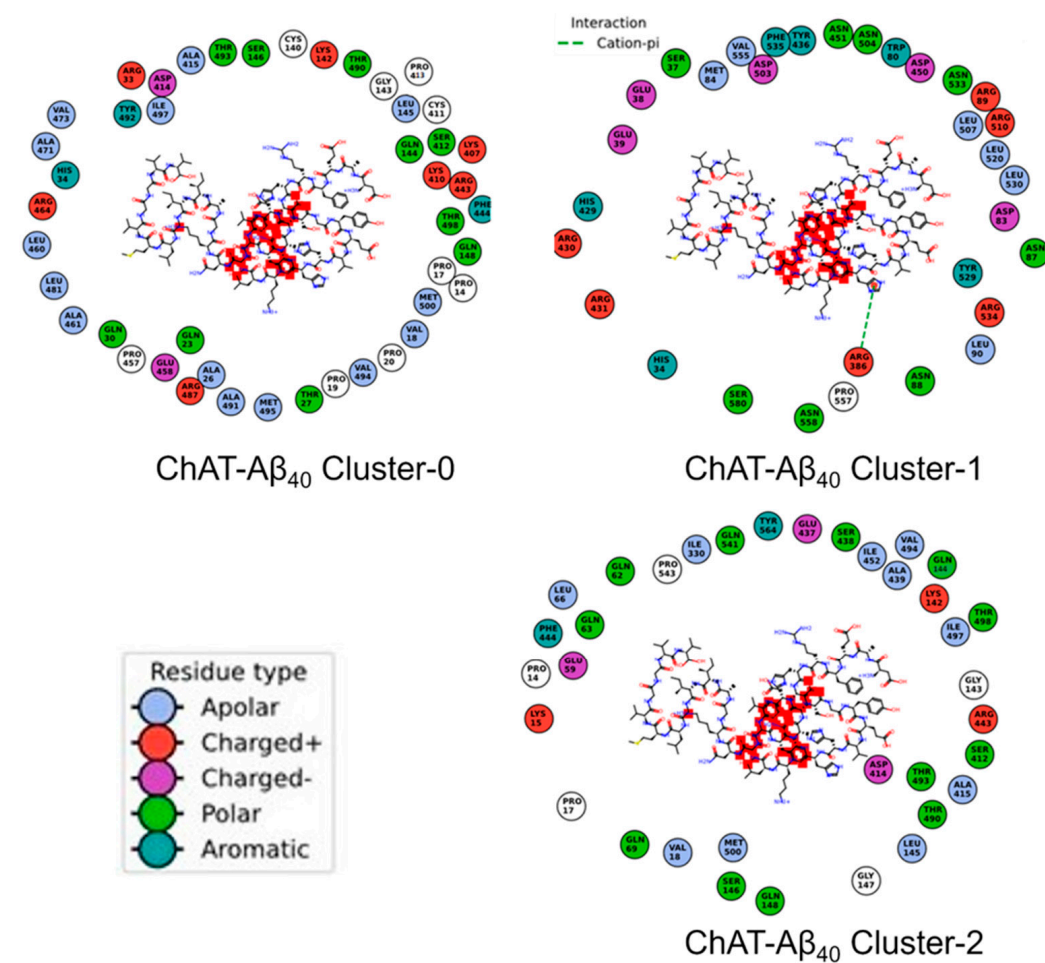


Figure 10. Contact maps between the ChAT protein and $A\beta_{40}$ peptides in the complexes. The amino acid residue types are given with the color codes as blue (Apolar), red ('+' charged), purple ('-' charged), light green (Polar), dark green (Aromatic).

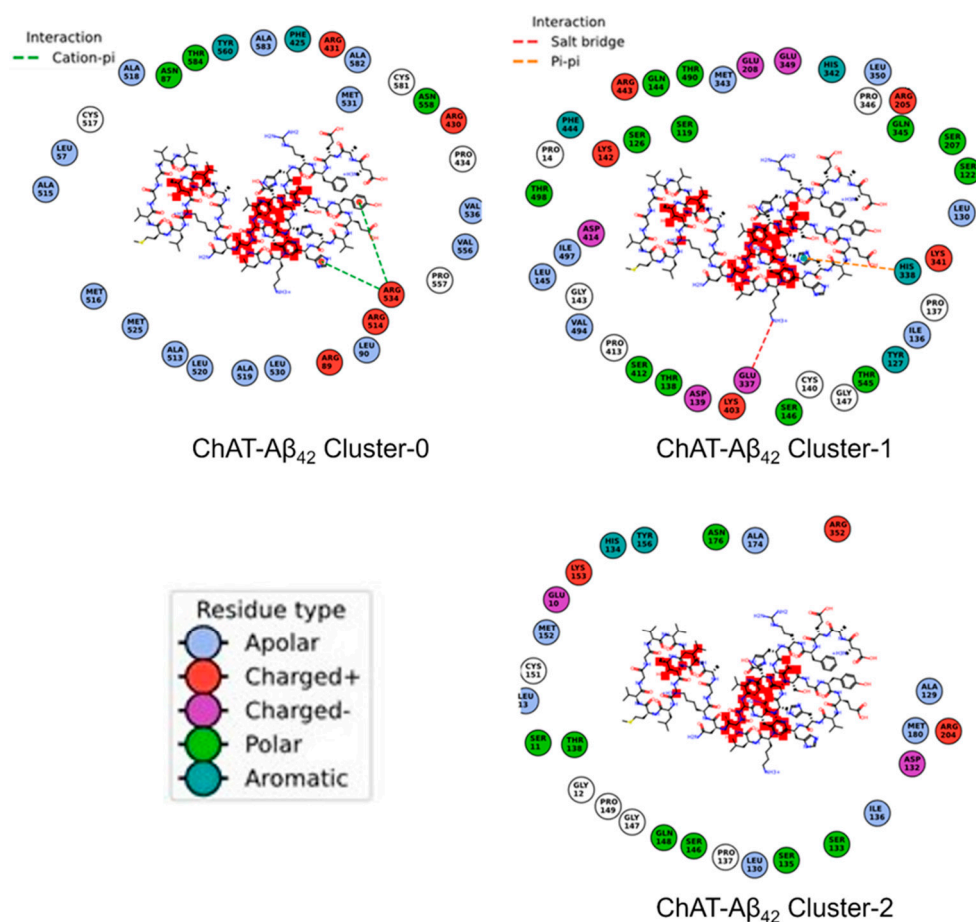


Figure 11. Contact maps between the ChAT protein and A β_{42} peptides in the complexes. The amino acid residue types are given with the color codes as blue (Apolar), red ('+' charged), purple ('-' charged), light green (Polar), dark green (Aromatic).

3. Discussion

Our previous report clearly revealed that mainly A β_{42} peptides potentiate the catalytic rate of ChAT by 20–30%. In contrast, A β_{40} potentiates ChAT activity in some analysis, but inhibits it in the others (compare Figures 1A and 1C). To shed light on such discrepancies, as well as to elucidate the molecular fingerprint of the interaction between A β peptides and ChAT governing the CPL activity of the A β peptides, we conducted the current investigation using two *in silico* approaches, namely a molecular docking and a 100 ns-long molecular dynamics (MD) simulation analysis.

Here, we show that the molecular docking analysis identified three high probability clusters for A β_{40} , and three for A β_{42} . Interestingly, molecular docking identified high-probability ChAT-A β complex clusters for both A β_{40} and A β_{42} that had overlapping binding sites with the mouth of the Choline/ACh entrance site of the ChAT catalytic tunnel, which is expected to inhibit rather than enhance ChAT catalytic efficiency. Nonetheless, we also identified binding clusters that blocked the ACoA/-CoA entrance site.

While the overlapping binding cluster of A β_{40} with the choline/ACh entrance site could explain the inconsistency observed for the mode of action of A β_{40} peptides on ChAT in the *in vitro* experiments, where in some experiments A β_{40} inhibited, and in others it enhanced ChAT activity. Yet, such an entrance-overlapping cluster fails to explain why A β_{42} did not exhibit this dual mode of action. Nonetheless, there were some differences that could shed light on this difference. (1) Molecular docking and MD analyses suggested that A β_{42} had two additional high probability clusters that did not overlap with the mouth of the choline/ACh catalytic tunnel of ChAT (compare Figures 2 and 9). (2) In addition, molecular docking analysis indicated that the A β_{42} had two clusters with a binding site

in close vicinity of the entrance of ACoA/-CoA into the catalytic tunnel (Figure 2G,H) of which cluster-1 seems to cover the entrance of ACoA/-CoA in Lowest Energy Minima conformer obtained from MD analysis (Figure 9P). In turn, such alternative bindings could mediate a positive effect on the substrate influx into the catalytic domain upon A β ₄₂ interaction that is absent in case of A β ₄₀, and thereby on the catalytic efficiency of ChAT, in a manner that we have previously reported for the interaction of A β with BuChE [13].

Of note, there are two fundamental differences that exist between the catalytic modes of cholinesterases (AChE and BuChE) and ChAT. Firstly, ChAT can act reversibly, meaning that it can both produce and breakdown ACh, while ChEs only degrade ACh. Thus, ChAT always produces two products: ACh and -CoA in the forward reaction but choline and Acetyl-CoA in the reverse reaction. Secondly, the rate-limiting step in the cycle of ACh synthesis is the release of -CoA from its binding site (that is why -CoA is reported to act as an inhibitor of ChAT at concentrations higher than 50 μ M) [30].

Overall, the following hypothetical explanations may account for the observed changes in the catalytic activity of ChAT in the presence of A β peptides as reported by us (Figure 1) and the conflicting reports by others. (1) Some of the binding clusters may indicate that binding of A β , in particular A β ₄₂, induces a conformational change in the enzyme structure, facilitating a faster release of -CoA from its binding sites and allowing the enzyme a faster re-entry into a new ACh cycle production. (2) Other *in silico* clusters may indicate that A β might reduce the reverse reaction of ChAT i.e., prevent the conversion of ACh and -CoA to choline and Acetyl-CoA. In other words, in these binding clusters, A β mainly directs the forward ACh production reaction. This could occur by favoring the entrance of Choline and/or Acetyl-CoA from their respective entrances or prevent/reduce the entrance of ACh and -CoA into the catalytic domain. (3) Given that both A β ₄₂ and A β ₄₀ are expected to be present together *in vivo*, the most likely scenario is that both alternative mechanisms are at work simultaneously, allowing A β ₄₂ to mainly act as ChAT potentiating ligand (CPL) by implementing both alternatives, while allowing A β ₄₀ to act as a weak CPL or a blocker of A β ₄₂ and ChAT activity. The net effect would be a controlled increase in ACh production in some situations but not in others. However, based on the current data, we can neither exclude nor confirm any of these scenarios, although the overall *in vitro* data favors the third alternative, as indicated by the data shown in Figure 1, where a biological 10:1 ratio of A β ₄₀ to A β ₄₂ resulted in ~15% CPL activity compared to ~25% for A β ₄₂ alone.

The fourth hypothetical explanation concerns with the possibility of dual A β binding or exclusion of binding. For instance, the binding of A β ₄₂ at the cluster-1 site seems to be excluding the binding of A β ₄₂ to the cluster-2 site but not the cluster-0 site (Figure 2F–H). This may increase the probability of simultaneous binding of two A β ₄₂ peptides at the opposite cluster-0 and -1 site (or -0 and -2) on ChAT protein (Figure 2F and 2G or 2F and 2H). In contrast, the binding sites for cluster-0 and cluster-1 for A β ₄₀ are too close to each other, which most likely could exclude the simultaneous binding of two A β ₄₀ peptides on the hAT protein (Figure 2B,C). As A β ₄₀ binds at cluster-1, but not at cluster -0 or -2, and completely blocking the entrance of choline/ACh into the catalytic tunnel, we can expect a 50% chance for either activation or inhibition, explaining the inconsistency in the activation of ChAT by A β ₄₀ peptides.

For the docking and molecular dynamics analysis, we randomly chose one out of several conformations for A β ₄₀ and A β ₄₂ structures that were present in PDB deposition. Nonetheless, the A β ₄₀ and A β ₄₂ peptides have disordered/unstructured N- and C-terminals and can exist in several different conformations as shown by structural NMR studies [27,28]. In addition, despite the successful docking analyses by ClusPro docking server in the prediction of the binding mode of A β peptides to ChAT, it should be mentioned that the analyses represented a rigid-body docking, which does not allow conformational changes during protein–protein interactions. To overcome these limitations, we performed an advanced 100 ns molecular dynamics simulation on the representative clusters. These molecular dynamics analyses not only confirmed the unstructured nature of C- and N-terminals in A β peptides, but also provided evidence that the ChAT-A β com-

plexes were stable, supporting a plausible mode of interaction between these two proteins. Overall, these *in silico* analyses strongly confirm a direct physical interaction between A β peptides and the ChAT protein, which further support our published *in vitro* enzyme kinetic analyses.

4. Materials and Methods

4.1. *In Silico* Analysis

4.1.1. Molecular Docking Studies

To reveal the probable interaction sites between A β peptides and ChAT protein, we performed *in silico* molecular docking studies using a similar strategy, as described earlier for A β peptides vs AChE and BuChE. [13] Briefly, the X-ray crystal structure of ChAT (PDB id: 2FY3) [31], and solution structures of A β_{42} (PDB id: 1IYT) [27] and A β_{40} (PDB id: 1BA4) [28] were downloaded from the RCSB protein data bank and examined thoroughly for any artifacts. For this docking analysis, we randomly chose one out of several conformations for A β_{40} and A β_{42} structures that were present in the PDB deposition for A β peptides.

The structures were further prepared using the protein structure preparation tool of SYBYL-X molecular modeling suite installed on Linux based Dell Precision T7610 workstation (Intel™ Xeon™ E5-2643 CPU @ 3.3 GHz; 16GB RAM, 2 TB hard disk). The protein preparation steps involved the addition of any missing hydrogens, deletion of water molecules, and energy minimization using the Powell method [32] with a Tripos force field.

Cluspro 2.0 [33–35], a fully automated protein-protein docking web server was used for the docking studies. The Cluspro docking involves three main steps. As the first step, PIPER, a Fast Fourier Transform correlation-based docking method is employed to obtain a set of solutions, which is then followed by clustering of the obtained solutions based on a hierarchical pairwise root mean squared deviation (RMSD) algorithm to retain near-native conformations and discard the unstable clusters as a second step. In the third and final step, the identified clusters are evaluated for their stability using the Monte Carlo method and further refinement was performed by using the medium range optimization method. The best models are selected based on the size of the clusters and the parameters generated by the 'Balanced' scoring function defined by a balance between the electrostatic, hydrophobic, and van der Waals forces.

4.1.2. Molecular Dynamics Simulations Analysis

Molecular dynamics study was performed using GROMACS 2020 and AMBER99SB-ILDN force field [36–39]. Briefly, the top scoring complexes were solvated in a cubic box simple point charge (SPC/E) water model keeping a distance of 1.0 nm between each side. Further, the system was solvated and ionized with Na⁺ and Cl[−] ions at a concentration of 100 mM to neutralize the system. The system was then minimized using the steepest descent algorithm until the maximum force became less than 1000 kJ/mol/nm. We used position restraining during the equilibration run using constant number, volume, and temperature (NVT) and isothermal-isobaric (NPT) ensemble for 1 ns each to avoid any distortion, which might happen during the equilibration step and make the system unstable. We used V-rescale temperature coupling [40] and Parrinello–Rahman pressure coupling [41] to maintain the system at 300 K temperature and 1 bar pressure along with a coupling constant of 0.1 picosecond (ps) for temperature and 2 ps for pressure. Position restraining was used during NVT and NPT ensemble simulations and the long-range electrostatic interactions and van der Waals interactions were calculated using the Particle mesh Ewald (PME) method [42] and the cut-off for short-range van der Waals was set to 1 nm. All bonds were constrained using LINCS algorithm [43] and the time step of the simulation was set to 0.002 ps. Finally, a 100 ns production simulation was performed, and carried out in triplicates under periodic boundary conditions. The final production simulation trajectory was analyzed quantitatively by calculating root means square deviation (RMSD), root mean square fluctuation (RMSF), radius of gyration (Rg), solvent accessible surface

area (sasa) and secondary structure analysis using rmsd, rmsf, gyrate, sasa and do_dssp functionalities, respectively. H-bond functionality was used to analyze the hydrogen bond formed between ChAT and A β peptides and also the hydrogen bond distance throughout the simulation time.

Protein molecules have entrenched movements that are mainly due to their complex association within their atomic motions, which are of utmost importance in regular conventional functioning of the protein. These internal motions of a protein molecules are difficult to interpret. Thus, PCA analysis was also carried out with the help of modules such as gmx covar and gmx ana eig available on GROMACS. The motion in MD trajectories was analyzed, which gives an insight into the crucial motions of the simulated system [44,45]. PCA was carried out for the ChAT-A β peptides complex using the gmx covar and gmx ana eig in two steps: (a) constructing the covariance matrix using the Backbone atoms and (b) diagonalization of the covariance matrix of the atomic coordinates. The relative motion of the complex system was obtained as the projection of the first two eigenvectors, which accounted for containing the maximum motion of the system. The eigenvectors are a representation of the direction of the motion, whereas eigenvalues represent the magnitude of motion along with the direction. On these projections, we can see the clusters of stable states. The overall flexibility of the ChAT-A β peptides complex was calculated by the trace of the diagonalized covariance matrix of the backbone atomic positional fluctuations. Moreover, the free-energy landscape was analyzed using the gmx sham module available on GROMACS, and the contact maps for the amino acid residue interactions between ChAT protein and A β peptides were evaluated to gain insight into the mechanism of how A β peptides interact with the ChAT protein.

5. Conclusions

In light of the failure of numerous A β -directed clinical drug trials in the AD field, it is now of utmost important that we should take a step back and focus more on understanding the native function of A β peptides and their involvement in AD-related cholinergic dysfunction. Here, we performed advanced in silico analyses (molecular docking and molecular simulation studies) to further understand the observed in vitro direct interacting mechanism between the key-cholinergic enzyme, ChAT and A β peptides [26]. The molecular docking analyses suggested three most probable binding clusters on ChAT for A β_{40} and A β_{42} . Interestingly, one binding cluster of each A β_{40} and A β_{42} overlapped the choline/ACh entrance site on the ChAT catalytic tunnel, which is expected to inhibit rather than enhance ChAT catalytic efficiency. The results of the molecular dynamics simulation studies clearly demonstrated that the ChAT-A β complexes were energetically stable despite the unstructured nature of C- and N-terminals in A β peptides and formed anticipated hydrogen bonds during simulated interaction studies. The present in silico analyses hence further reinforce our published in vitro ChAT-A β interaction study. Overall, our findings provide new information and shed light on the potential unexplored complex molecular crosstalk between A β and the enzymatic machinery involved in maintaining cellular, synaptic, and extra-synaptic ACh homeostasis [13,26]. We expect these insights to open new avenues for both a proper understanding of the pathophysiological role of A β peptides related specifically to the cholinergic dysfunction in AD, as well as for developing a new class of cholinergic enhancing drugs that mimic the CPL activity of A β_{42} peptides for the treatment of the cholinergic deficit seen in AD-related dementias and the neuromotor disorders such as ALS.

Supplementary Materials: The Supplementary Materials can be downloaded at: <https://www.mdpi.com/article/10.3390/ijms23116073/s1>.

Author Contributions: The concept and design of the study was completed by R.K. and T.D.-S. In silico analyses was completed by R.K. and A.T.B. A.K., R.K., A.T.B. and T.D.-S. analyzed the data. A.K. wrote the first draft of the manuscript. All authors have read and agreed to the published version of the manuscript.

Funding: This study was supported by grants from Demensfonden; Åhlén-Foundation; Olle Engkvist Byggmästare Foundation; Foundation for Old Servants (Stifelsen Gamla Tjänarinnor); Magnus Bergvalls Foundation; Loo & Hans Osterman Foundation; KI Foundations; KI Geriatrics Foundations; Petra and Augusta Hedlund Foundation; Lindhés Advokatbyrå AB Stiftelser; Gunvor and Josef Anérs Foundation; The Lars Hierta Memorial Foundation; Gun and Bertil Stohnes Foundation; Foundation for Sigurd & Elsa Goljes Memory; Tore Nilsson Foundation; Alzheimer Association, USA (2016-NIRG-391599), the Swedish Research Council (project no 2016-01806), grant from the Swedish state under the agreement between the Swedish government and the county councils, the ALF-agreement (ALF Med N 20200330) and Science Engineering & Research Board (SERB) (start-up grant no. SRG/2021/000415).

Institutional Review Board Statement: Not applicable.

Informed Consent Statement: Not applicable.

Data Availability Statement: The trajectories and topology files for all six clusters obtained after molecular dynamics simulation are archived on Zenodo, doi: 10.5281/zenodo.5912821.

Acknowledgments: The computations/simulations/ were performed on resources provided by the Swedish National Infrastructure for Computing (SNIC) at National Supercomputer Centre at Linköping University (NSC). The support and the resources provided by ‘PARAM Shivay Facility’ under the National Supercomputing Mission, Government of India at the Indian Institute of Technology (BHU), Varanasi are gratefully acknowledged. E.L. and C.U.L. provided critical input during the preparation of the manuscript.

Conflicts of Interest: The authors declare no conflict of interest.

References

1. Selkoe, D.J. Alzheimer’s disease: Genes, proteins, and therapy. *Physiol. Rev.* **2001**, *81*, 741–766. [[CrossRef](#)] [[PubMed](#)]
2. Goedert, M.; Spillantini, M.G. A century of Alzheimer’s disease. *Science* **2006**, *314*, 777–781. [[CrossRef](#)] [[PubMed](#)]
3. Brion, J.P. Neurofibrillary tangles and Alzheimer’s disease. *Eur. Neurol.* **1998**, *40*, 130–140. [[CrossRef](#)] [[PubMed](#)]
4. Price, D.L. New Perspectives on Alzheimer’s Disease. *Annu. Rev. Neurosci.* **1986**, *9*, 489–512. [[CrossRef](#)] [[PubMed](#)]
5. DeKosky, S.T.; Scheff, S.W. Synapse loss in frontal cortex biopsies in Alzheimer’s disease: Correlation with cognitive severity. *Ann. Neurol.* **1990**, *27*, 457–464. [[CrossRef](#)] [[PubMed](#)]
6. Li, X.; Yu, B.; Sun, Q.; Zhang, Y.; Ren, M.; Zhang, X.; Li, A.; Yuan, J.; Madisen, L.; Luo, Q.; et al. Generation of a whole-brain atlas for the cholinergic system and mesoscopic projectome analysis of basal forebrain cholinergic neurons. *Proc. Natl. Acad. Sci. USA* **2018**, *115*, 415–420. [[CrossRef](#)]
7. Wurtman, R.J. Choline metabolism as a basis for the selective vulnerability of cholinergic neurons. *Trends Neurosci.* **1992**, *15*, 117–122. [[CrossRef](#)]
8. Rylett, R.; Ball, M.; Colhoun, E. Evidence for high affinity choline transport in synaptosomes prepared from hippocampus and neocortex of patients with Alzheimer’s disease. *Brain Res.* **1983**, *289*, 169–175. [[CrossRef](#)]
9. Quirion, R. Cholinergic markers in Alzheimer disease and the autoregulation of acetylcholine release. *J. Psychiatry Neurosci.* **1993**, *18*, 226–234.
10. Wyss-Coray, T.; McConlogue, L.; Kindy, M.; Schmidt, A.M.; Du Yan, S.; Stern, D.M. Key signaling pathways regulate the biological activities and accumulation of amyloid-beta. *Neurobiol. Aging* **2001**, *22*, 967–973. [[CrossRef](#)]
11. Dineley, K.T.; Westerman, M.; Bui, D.; Bell, K.; Ashe, K.H.; Sweatt, J.D. Beta-amyloid activates the mitogen-activated protein kinase cascade via hippocampal alpha7 nicotinic acetylcholine receptors: In vitro and in vivo mechanisms related to Alzheimer’s disease. *J. Neurosci.* **2001**, *21*, 4125–4133. [[CrossRef](#)] [[PubMed](#)]
12. Atkins, C.; Selcher, J.C.; Petraitis, J.J.; Trzaskos, J.M.; Sweatt, J.D. The MAPK cascade is required for mammalian associative learning. *Nat. Neurosci.* **1998**, *1*, 602. [[CrossRef](#)] [[PubMed](#)]
13. Kumar, R.; Nordberg, A.; Darreh-Shori, T. Amyloid-beta peptides act as allosteric modulators of cholinergic signalling through formation of soluble BAβACs. *Brain* **2016**, *139 Pt 1*, 174–192. [[CrossRef](#)] [[PubMed](#)]
14. Kar, S.; Seto, D.; Gaudreau, P.; Quirion, R. Beta-amyloid-related peptides inhibit potassium-evoked acetylcholine release from rat hippocampal slices. *J. Neurosci.* **1996**, *16*, 1034–1040. [[CrossRef](#)] [[PubMed](#)]
15. Pedersen, W.A.; Kloczewiak, M.A.; Blusztajn, J.K. Amyloid beta-protein reduces acetylcholine synthesis in a cell line derived from cholinergic neurons of the basal forebrain. *Proc. Natl. Acad. Sci. USA* **1996**, *93*, 8068–8071. [[CrossRef](#)]
16. Hoshi, M.; Takashima, A.; Murayama, M.; Yasutake, K.; Yoshida, N.; Ishiguro, K.; Hoshino, T.; Imahori, K. Nontoxic amyloid beta peptide 1–42 suppresses acetylcholine synthesis. Possible role in cholinergic dysfunction in Alzheimer’s disease. *J. Biol. Chem.* **1997**, *272*, 2038–2041. [[CrossRef](#)]
17. Pedersen, W.A.; Blusztajn, J.K. Characterization of the acetylcholine-reducing effect of the amyloid-beta peptide in mouse SN56 cells. *Neurosci. Lett.* **1997**, *239*, 77–80. [[CrossRef](#)]

18. Kar, S.; Issa, A.M.; Seto, D.; Auld, D.S.; Collier, B.; Quirion, R. Amyloid beta-peptide inhibits high-affinity choline uptake and acetylcholine release in rat hippocampal slices. *J. Neurochem.* **1998**, *70*, 2179–2187. [[CrossRef](#)]
19. Satoh, Y.; Hirakura, Y.; Shibayama, S.; Hirashima, N.; Suzuki, T.; Kirino, Y. Beta-amyloid peptides inhibit acetylcholine release from cholinergic presynaptic nerve endings isolated from an electric ray. *Neurosci. Lett.* **2001**, *302*, 97–100. [[CrossRef](#)]
20. Nunes-Tavares, N.; Santos, L.E.; Stutz, B.; Brito-Moreira, J.; Klein, W.L.; Ferreira, S.T.; de Mello, F.G. Inhibition of Choline Acetyltransferase as a Mechanism for Cholinergic Dysfunction Induced by Amyloid-beta Peptide Oligomers. *J. Biol. Chem.* **2012**, *287*, 19377–19385. [[CrossRef](#)]
21. Nitta, A.; Itoh, A.; Hasegawa, T.; Nabeshima, T. Beta-Amyloid protein-induced Alzheimer's disease animal model. *Neurosci. Lett.* **1994**, *170*, 63–66. [[CrossRef](#)]
22. Giovannelli, L.; Casamenti, F.; Scali, C.; Bartolini, L.; Pepeu, G. Differential effects of amyloid peptides beta-(1-40) and beta-(25-35) injections into the rat nucleus basalis. *Neuroscience* **1995**, *66*, 781–792. [[CrossRef](#)]
23. Harkany, T.; Lengyel, Z.; Soos, K.; Penke, B.; Luiten, P.G.; Gulya, K. Cholinotoxic effects of beta-amyloid (1-42) peptide on cortical projections of the rat nucleus basalis magnocellularis. *Brain Res.* **1995**, *695*, 71–75. [[CrossRef](#)]
24. Itoh, A.; Nitta, A.; Nadai, M.; Nishimura, K.; Hirose, M.; Hasegawa, T.; Nabeshima, T. Dysfunction of cholinergic and dopaminergic neuronal systems in beta-amyloid protein-infused rats. *J. Neurochem.* **1996**, *66*, 1113–1117. [[CrossRef](#)] [[PubMed](#)]
25. Maurice, T.; Lockhart, B.P.; Privat, A. Amnesia induced in mice by centrally administered beta-amyloid peptides involves cholinergic dysfunction. *Brain Res.* **1996**, *706*, 181–193. [[CrossRef](#)]
26. Kumar, A.; Lana, E.; Kumar, R.; Lithner, C.U.; Darreh-Shori, T. Soluble Aβ42 Acts as Allosteric Activator of the Core Cholinergic Enzyme Choline Acetyltransferase. *Front. Mol. Neurosci.* **2018**, *11*, 327. [[CrossRef](#)]
27. Crescenzi, O.; Tomaselli, S.; Guerrini, R.; Salvadori, S.; D'Ursi, A.M.; Temussi, P.A.; Picone, D. Solution structure of the Alzheimer amyloid beta-peptide (1-42) in an apolar microenvironment. Similarity with a virus fusion domain. *Eur. J. Biochem.* **2002**, *269*, 5642–5648. [[CrossRef](#)]
28. Coles, M.; Bicknell, W.; Watson, A.A.; Fairlie, D.P.; Craik, D.J. Solution structure of amyloid beta-peptide(1-40) in a water-micelle environment. Is the membrane-spanning domain where we think it is? *Biochemistry* **1998**, *37*, 11064–11077. [[CrossRef](#)]
29. Hong, L.; Lei, J. Scaling law for the radius of gyration of proteins and its dependence on hydrophobicity. *J. Polym. Sci. Part. B Polym. Phys.* **2009**, *47*, 207–214. [[CrossRef](#)]
30. Sastry, B.V.; Henderson, G.I. Kinetic mechanisms of human placental choline acetyltransferase. *Biochem. Pharm.* **1972**, *21*, 787–802. [[CrossRef](#)]
31. Kim, A.-R.; Rylett, R.J.; Shilton, B.H. Substrate binding and catalytic mechanism of human choline acetyltransferase. *Biochemistry* **2006**, *45*, 14621–14631. [[CrossRef](#)] [[PubMed](#)]
32. Wang, R.; Lu, Y.; Wang, S. Comparative evaluation of 11 scoring functions for molecular docking. *J. Med. Chem.* **2003**, *46*, 2287–2303. [[CrossRef](#)] [[PubMed](#)]
33. Kozakov, D.; Hall, D.R.; Xia, B.; Porter, K.A.; Padohny, D.; Yueh, C.; Beglov, D.; Vajda, S. The ClusPro web server for protein-protein docking. *Nat. Protoc.* **2017**, *12*, 255–278. [[CrossRef](#)] [[PubMed](#)]
34. Kozakov, D.; Beglov, D.; Bohnuud, T.; Mottarella, S.E.; Xia, B.; Hall, D.R.; Vajda, S. How good is automated protein docking? *Proteins* **2013**, *81*, 2159–2166. [[CrossRef](#)]
35. Kozakov, D.; Brenke, R.; Comeau, S.R.; Vajda, S. PIPER: An FFT-based protein docking program with pairwise potentials. *Proteins* **2006**, *65*, 392–406. [[CrossRef](#)]
36. Smith, M.D.; Rao, J.S.; Segelken, E.; Cruz, L. Force-field induced bias in the structure of Aβ21–30: A comparison of OPLS, AMBER, CHARMM, and GROMOS force fields. *J. Chem. Inf. Model.* **2015**, *55*, 2587–2595. [[CrossRef](#)]
37. Somavarapu, A.K.; Keep, K.P. The dependence of amyloid-β dynamics on protein force fields and water models. *ChemPhysChem* **2015**, *16*, 3278–3289. [[CrossRef](#)]
38. Jämbeck, J.P.M.; Lyubartsev, A.P. An extension and further validation of an all-atomistic force field for biological membranes. *J. Chem. Theory Comput.* **2012**, *8*, 2938–2948. [[CrossRef](#)]
39. Pacheco, M.C.; Strodel, B. Comparison of force fields for Alzheimer's A: A case study for intrinsically disordered proteins. *Protein Sci.* **2017**, *26*, 174–185. [[CrossRef](#)]
40. Bussi, G.; Donadio, D.; Parrinello, M. Canonical sampling through velocity rescaling. *J. Chem. Phys.* **2007**, *126*, 014101. [[CrossRef](#)]
41. Parrinello, M.; Rahman, A. Polymorphic transitions in single crystals: A new molecular dynamics method. *J. Appl. Phys.* **1981**, *52*, 7182–7190. [[CrossRef](#)]
42. Essmann, U.; Perera, L.; Berkowitz, M.L.; Darden, T.; Lee, H.; Pedersen, L.G. A smooth particle mesh Ewald method. *J. Chem. Phys.* **1995**, *103*, 8577–8593. [[CrossRef](#)]
43. Hess, B.; Bekker, H.; Berendsen, H.J.C.; Fraaije, J.G.E.M. LINCS: A linear constraint solver for molecular simulations. *J. Comput. Chem.* **1997**, *18*, 1463–1472. [[CrossRef](#)]
44. Daidone, I.; Amadei, A. Essential dynamics: Foundation and applications. *Wiley Interdiscip. Rev. Comput. Mol. Sci.* **2012**, *2*, 762–770. [[CrossRef](#)]
45. Buslaev, P.; Mustafin, K.; Gushchin, I. Principal component analysis highlights the influence of temperature, curvature and cholesterol on conformational dynamics of lipids. *Biochim. Biophys. Acta BBA-Biomembr.* **2020**, *1862*, 183253. [[CrossRef](#)]